# Mass Spectrometry-Based Pipeline for Identifying RNA Modifications Involved in a Functional Process: Application to Cancer Cell Adaptation

Amandine Amalric, Aurore Attina, Amandine Bastide, Marion Buffard, Stéphanie Mateus, Chris Planque, Eric Rivals, Christophe Hirtz, Alexandre David

analytical chemistry



pubs.acs.org/ac
Article

# Mass Spectrometry-Based Pipeline for Identifying RNA Modifications Involved in a Functional Process: Application to Cancer Cell Adaptation

Amandine Amalric,[‖] Aurore Attina,[‖] Amandine Bastide, Marion Buffard, Stéphanie Mateus, Chris Planque, Eric Rivals, Christophe Hirtz,* and Alexandre David*

Cite This: *Anal. Chem.* 2024, 96, 1825−1833
Read Online



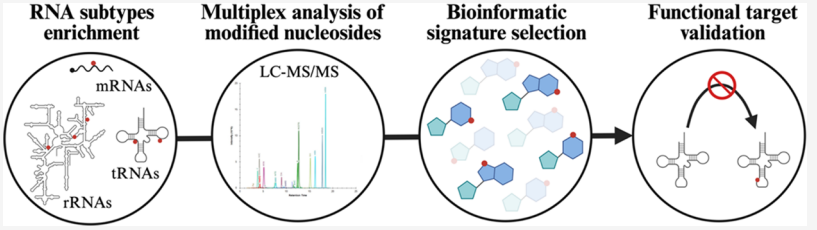


**ABSTRACT:** Cancer onset and progression are known to be regulated by genetic and epigenetic events, including RNA modifications (a.k.a. epitranscriptomics). So far, more than 150 chemical modifications have been described in all RNA subtypes, including messenger, ribosomal, and transfer RNAs. RNA modifications and their regulators are known to be implicated in all steps of post-transcriptional regulation. The dysregulation of this complex yet delicate balance can contribute to disease evolution, particularly in the context of carcinogenesis, where cells are subjected to various stresses. We sought to discover RNA modifications involved in cancer cell adaptation to inhospitable environments, a peculiar feature of cancer stem cells (CSCs). We were particularly interested in the RNA marks that help the adaptation of cancer cells to suspension culture, which is often used as a surrogate to evaluate the tumorigenic potential. For this purpose, we designed an experimental pipeline consisting of four steps: (1) cell culture in different growth conditions to favor CSC survival; (2) simultaneous RNA subtype (mRNA, rRNA, tRNA) enrichment and RNA hydrolysis; (3) the multiplex analysis of nucleosides by LC-MS/MS followed by statistical/bioinformatic analysis; and (4) the functional validation of identified RNA marks. This study demonstrates that the RNA modification landscape evolves along with the cancer cell phenotype under growth constraints. Remarkably, we discovered a short epitranscriptomic signature, conserved across colorectal cancer cell lines and associated with enrichment in CSCs. Functional tests confirmed the importance of selected marks in the process of adaptation to suspension culture, confirming the validity of our approach and opening up interesting prospects in the field.



## INTRODUCTION

The development of omics technologies, such as next-generation sequencing and mass spectrometry, has spurred nucleic acid research growth and revealed unsuspected complexity, specifically in the RNA field. Besides its canonical function as the carrier and decoder of genetic information, RNA catalyzes and regulates several biochemical reactions.[1] Such structural and functional diversity and flexibility require the deposition of various chemical modifications along the RNA sequence. Until now, more than 150 RNA marks have been described in all RNA subtypes: messenger RNA (mRNA), transfer RNA (tRNA), ribosomal RNA (rRNA), and other noncoding RNAs.[2] Most of them are found on multiple RNA subtypes, while some are distinctive of specific RNA subtypes.[3−6] RNA modifications are implicated in all steps of post-transcriptional regulation, encompassing splicing, stability, storage, and translation.[7] Their dynamics are orchestrated by the coordinated actions of a set of proteins named writers, readers, and erasers. Any dysregulation of this complex, yet delicate, balance can contribute to disease development including cancer.[3,8]

Cancer onset and evolution typically result from the accumulation of various molecular aberrations comprising genetic and epigenetic alterations.[9,10] The identification of genomic, transcriptomic, and epigenomic abnormalities is critical for precision oncology in many cancers, both to establish molecular subtypes and to offer appropriate treat-

Received: June 16, 2023
Revised: December 19, 2023
Accepted: December 19, 2023
Published: January 26, 2024

ment.[11−13] Likewise, the RNA mark landscape evolves along with tumor progression and represents a novel source of biomarkers for personalized medicine.[14] To illustrate this principle, our group has recently uncovered "epitranscriptomic signatures" from glioma patients' cohorts that could be exploited to guide glioma/glioblastoma diagnosis with unmet accuracy.[15] Far from being mere passengers in the tumorigenic process, several of these marks participate in cancer adaptation to conventional treatments and inhospitable environment.[16−19] For instance, recent reports show that a dysregulation of 5-methylcytidine ($m^5C$) players is associated with either oncogenic or tumor-suppressive functions according to cellular context.[20,21] The identification of RNA marks driving cancer cell adaptation to inhospitable environment and conventional treatment is essential to design appropriate therapeutic strategies, as emphasized by a growing drug discovery effort in the field.[22] Yet, the use of sequencing data is unsuitable for this purpose, as the regulation of these marks is subject to various post-transcriptional parameters, some of which are inherent to any subcellular enzymatic system.[23,24] Target(s) discovery steps necessitate the implementation of a dedicated pipeline that would allow the accurate quantification of RNA marks on isolated RNA species.

Cell adaptation is a peculiar feature of cancer stem cells (CSCs), a minor subpopulation of tumor cells that display stem-like traits, as well as tremendous chemoresistance and tumor initiation potential.[25] Suspension culture promotes the CSC phenotype and the formation of microtumor-like spheroids (colonospheres in the case of colorectal cancer, CRC) starting from a single cancer progenitor cell (19). As such, the sphere-forming ability (SFA) reflects the tumorigenic potential of solid tumors. Previously, we focused our attention on $N^6$-methyladenosine ($m^6A$) and performed a SFA-based screening limited to $m^6A$ writers. This approach allowed us to identify $N^6$,2′-O-dimethyladenosine ($m^6A_m$), adjacent to the mRNA cap, as a RNA mark involved in the acquisition of stemlike properties in colorectal cancer cells.[23]

In this study, we aimed to identify other RNA marks potentially involved in cancer cell adaptation to environmental changes. To fulfill this purpose, we designed a dedicated experimental pipeline comprising RNA subtype isolation (mRNA, rRNA, tRNA) and RNA modification quantification by liquid chromatography coupled with tandem mass spectrometry (LC-MS/MS) and statistical/bioinformatic analysis. We applied this method to compare cells from CSC-enriched culture to more differentiated cells grown in monolayer culture. As expected, the RNA subtypes displayed distinctive RNA mark profiles. We could demonstrate that the epitranscriptomic landscape evolved along with the culture condition, uncovering chemical patterns associated with the suspension culture condition and conserved across colorectal cell line. Finally, functional assays carried out on a short list of tRNA marks were able to confirm their importance on cell adaptation to suspension culture, thereby establishing the validity of our approach.

## EXPERIMENTAL SECTION

**Cell Culture.** SW620 (ATCC CCL-227) is a commercially available CRC line derived from a metastatic human tumor, and CRC1 is a patient-derived CRC line derived from a primary human tumor.[26] Cells were maintained at 37 °C under a humidified atmosphere in 5% $CO_2$ in high glucose DMEM medium (Gibco) supplemented with 10% FCS (Eurobio) and 2 mM glutamine or in M11 medium (DMEM/F12 (1:1) Glutamax medium (Gibco), N2 Supplement (Gibco), Glucose 0.3%, insulin 20 μg/mL, hBasic-FGF 10 ng/mL, and hEGF 20 ng/mL). For monolayer or "2D" culture, $4 \times 10^6$ cells were seeded in 15 mL of high glucose DMEM or M11 medium into 150 mm Petri dishes and cultured for 3 days (1 plate per condition). For suspension or "3D" culture, $3 \times 10^5$ cells in 30 mL of M11 medium (10 cells/μL) were seeded in a T75 polyheme-coated flask and cultured for 7 days (3 flasks per condition).

Patient-derived colon cancer cell lines (CRC1) were derived from colorectal cancer surgeries provided by CHU-Carremeau (Nîmes, France, ClinicalTrial.gov Identifier# NCT01577511) within an approved protocol by the French Ethics Committee: CPP (Comité de Protection des Personnes) Sud Méditerranée III. We have complied with all relevant ethical regulations for work with human participants, and informed written consent was obtained for all of the patients.

**RNA Processing.** *Total RNA Extraction.* The extraction of total RNA was achieved using the TRI reagent (Sigma, T9424), according to the manufacturer's instructions.

*mRNA Isolation.* mRNA was isolated from 50 μg of total RNA using the GenElute mRNA purification kit (Sigma, MRN70), according to the manufacturer's protocol. Two successive rounds were performed, and mRNA was eluted in 100 μL of RNase-free water.

*rRNA Isolation.* To obtain rRNA, total RNA samples were subjected to one round of the GenElute mRNA purification kit and the RNA from the flow-through (containing rRNA) was precipitated (refer to RNA precipitation) and resuspended with 20 μL of RNase-free water. The RNA samples were then separated by electrophoresis in a 1% agarose gel, stained with SYBR Safe (Invitrogen, S33102), and 28S and 18S rRNA bands were excised under ultraviolet light and purified using the NucleoSpin gel extraction kit (Macherey-Nagel, 740609).

*tRNA Isolation.* To obtain tRNA, 10 μg of total RNA was separated by electrophoresis in a Novex TBE-Urea 10% polyacrylamide gel (Invitrogen, EC6875BOX). After SYBR Gold (Invitrogen, S11494) staining, the tRNA bands were excised under ultraviolet light and the RNA was eluted from the acrylamide gel. Briefly, using filter cartridges (Invitrogen, 10051G2), the gel piece was crushed by centrifugation (16,100*g* for 5 min at 4 °C) in a prepunched 0.5 mL tube, placed in a 1.5 mL tube, and then RNA was eluted with 400 μL of RNA elution buffer (0.3% NaCl, 1 mM EDTA) overnight at 4 °C under agitation. The eluted RNA was recovered after centrifugation through a filter cartridge (Invitrogen, 10051G2) at 16,100*g* for 4 min at 4 °C and precipitation (refer to RNA precipitation), and resuspended in 20 μL of RNase-free water.

**RNA Precipitation.** RNA contained in solution was precipitated by adding 2 volumes of 100% ethanol, 1/10 volume of 3 M sodium acetate pH 5.5 (Invitrogen, AM9740), and 2 μL of glycogen (Invitrogen, AM9510).

After precipitating overnight at −20 °C, the RNA was pelleted by centrifugation at 12,000*g* for 30 min at 4 °C. The pellet was washed with 75% ethanol and centrifuged at 7,500*g* for 10 min at 4 °C. The air-dried pellet was then resuspended in RNase-free water.

**RT-qPCR.** For RT-qPCR analyses, 200 ng of RNA was reverse-transcribed into cDNA using random hexamers (Invitrogen, N8080127) and 1 U of MML-V reverse transcriptase (Invitrogen, 28025013). Quantitative gene expression was performed using SYBR Green master mix


https://doi.org/10.1021/acs.analchem.3c02635
Anal. Chem. 2024, 96, 1825−1833

(Roche, 04707516001) on a LightCycler 480 Instrument (Roche). The primer sequences are provided in the Supporting Information (Table S1).

**RNA Digestion.** 200 ng of RNA was enzymatically hydrolyzed to nucleosides. The RNA samples were digested with 0.5 mU of phosphodiesterase I from *Crotalus adamanteus* venom (Sigma, P3243) and 0.5 U of alkaline phosphatase from calf intestine (Sigma, SRP6549) for 2 h at 37 °C in 100 mM $NH_4OAc$. The samples were filtrated with 0.22 μm filters (Millex-GV, Millipore, SLGVR04NL). 5 μL of each sample was injected in triplicate for LC-MS/MS analysis.

**Nucleoside Mass Spectrometry Analysis.** *Nucleoside Standards and Chemical Products.* Nucleoside standards are commercially available from various suppliers like Biosynth Carbosynth (Staad, Switzerland), Toronto Research Chemicals (Toronto, Canada), or Sigma-Aldrich (Steinheim, Germany).

Acetonitrile (0001204101BS, CAS: 75-05-8), water (0023214102BS, CAS: 7732-18-5), and ammonium acetate (001244153BS, CAS: 631-61-8) were purchased from Biosolve Chimie (Dieuze, France) and glacial acetic acid (5330010050, CAS: 64-19-7) was purchased from Sigma-Aldrich (Steinheim, Germany). All chemical products were purchased by grade LC-MS.

*LC Method.* The nucleosides were separated by reverse-phase ultraperformance liquid chromatography (Nexera LC-40 system, Shimadzu) on a C18 column (Synergi Fusion-RP; 4 μm particle size, 250 mm × 2 mm, 80 Å, Phenomenex, 00G-4424-B0). The mobile phases consisted of 5 mM ammonium acetate pH 5.3 (solvent A) and pure acetonitrile (solvent B). The 30 min elution gradient started with 100% phase A followed by a linear gradient to 8% solvent B at 13 min. Solvent B was increased further to 40% over 10 min. After 2 min, solvent B was decreased back to 0% at 25.5 min. Initial conditions were regenerated by rinsing with 100% solvent A for an additional 4.5 min. The flow rate was 0.4 mL/min, and the column temperature was 35 °C.

*MRM Method.* The nucleoside detection was performed using a Shimadzu TripleQuad NX8060 in the positive ion mode. The ESI source settings were set as described in Table 1. The multiple reaction monitoring (MRM) transitions used for the detection of 38 targets and the linearity curves are shown in the Supporting Information (Table S2 and Figure S3).

**Table 1. ESI Instrument Settings Used for the Detection of All Nucleosides**

| parameters | setting |
|---|---|
| nebulizing gas flow | 3 L/min |
| heating gas flow | 10 L/min |
| interface temperature | 350 °C |
| DL temperature | 225 °C |
| heat block temperature | 400 °C |
| drying gas flow | 3 L/min |
| focus voltage | 2 kV |
| interface voltage | 0.5 kV |
| CID gas | 250 kPa |

MS was operated in the dynamic MRM mode with a retention time window of 3 min and a maximum cycle time set at 497 ms.

**Statistical Analysis.** The peak areas were analyzed and extracted using Skyline 21.2.0 software. To normalize them, we computed the ratio between the total area of the modified nucleoside and that of the unmodified nucleoside (uridine, U). Principal component analysis (PCA) was performed for the decomposition and visualization of a data matrix composed of the ratio described above using the package FactoMineR version 2.4 with R software.[27] An imputation of data was performed, if necessary, with a k-dimensional PCA model. PCA is described with two complementary graphs: one to represent individuals and one to represent variables. In the graph of individuals, each axis is described with the percentage of the explained variance. The graph of variables represents the correlation of each quantitative variable with the described dimensions. The more correlated a variable is to one dimension, the closer its $cos^2$ value is to 1. We term this $cos^2$ value the importance of the variable (a term coming from the machine learning terminology).

**Bioinformatic Signature Selection.** In order to reduce the signature, we combined the importance value of nucleosides (coming from PCA, see above) and the Pearson correlation coefficient between the pairs of nucleosides. Using Pearson correlation threshold $|r| > 0.98$, we reduced information redundancy in the final signature. When nucleoside variations are correlated, we select the nucleoside with the largest importance to be representative of the others. When one represented nucleoside is correlated with the other nucleoside(s) than the represented ones, then we keep the extra nucleoside with the largest importance. Then, we also select the nucleosides that are not correlated with any other when their importance value is superior to 0.93 (see Figure S4 for more details on the procedure).

**Protein Extraction and Western Blot.** Protein extraction and Western blot have been performed as previously described.[23] Table S5 provides the dilution and references for commercial antibodies.

**Transfection, Sphere Formation, and Proliferation Assays.** The transfection of the siRNA duplex, sphere formation, and proliferation assays have been performed as previously described.[23] Table S6 provides the siRNA sequences.

Figures were created using BioRender.com.

## RESULTS AND DISCUSSION

**RNA Modification Profile Is Specific to Each RNA Subtype.** In order to identify RNA modifications potentially involved in the SFA, we designed an experimental pipeline comprising four steps: (1) cell culture in distinct growth conditions; (2) simultaneous RNA subtype (mRNA, rRNA, and tRNA) enrichment and enzymatic processing; (3) multiplex analysis of nucleosides by LC-MS/MS followed by statistical/bioinformatic study; and (4) functional validation of identified mark(s) of interest (Figure 1A). The RNA subtypes were purified from the SW620 colorectal cancer cell line, and the enrichment procedure was assessed by quantitative RT-PCR (Table S7 and Figures S8−S10) prior to LC-MS/MS analysis.

We have previously developed a method allowing the multiplex analysis of RNA modifications.[23] Our LC-MS/MS method was set up to detect the four unmodified nucleosides (A, C, U, and G) and 34 modified nucleosides. From SW620 RNA samples grown on monolayer culture with DMEM medium, we were able to detect and quantify 28 RNA modifications in total RNA and tRNA, 19 in mRNA, and 21 in rRNA (Figure 1B). As anticipated, tRNA contributes to the


https://doi.org/10.1021/acs.analchem.3c02635
Anal. Chem. 2024, 96, 1825−1833

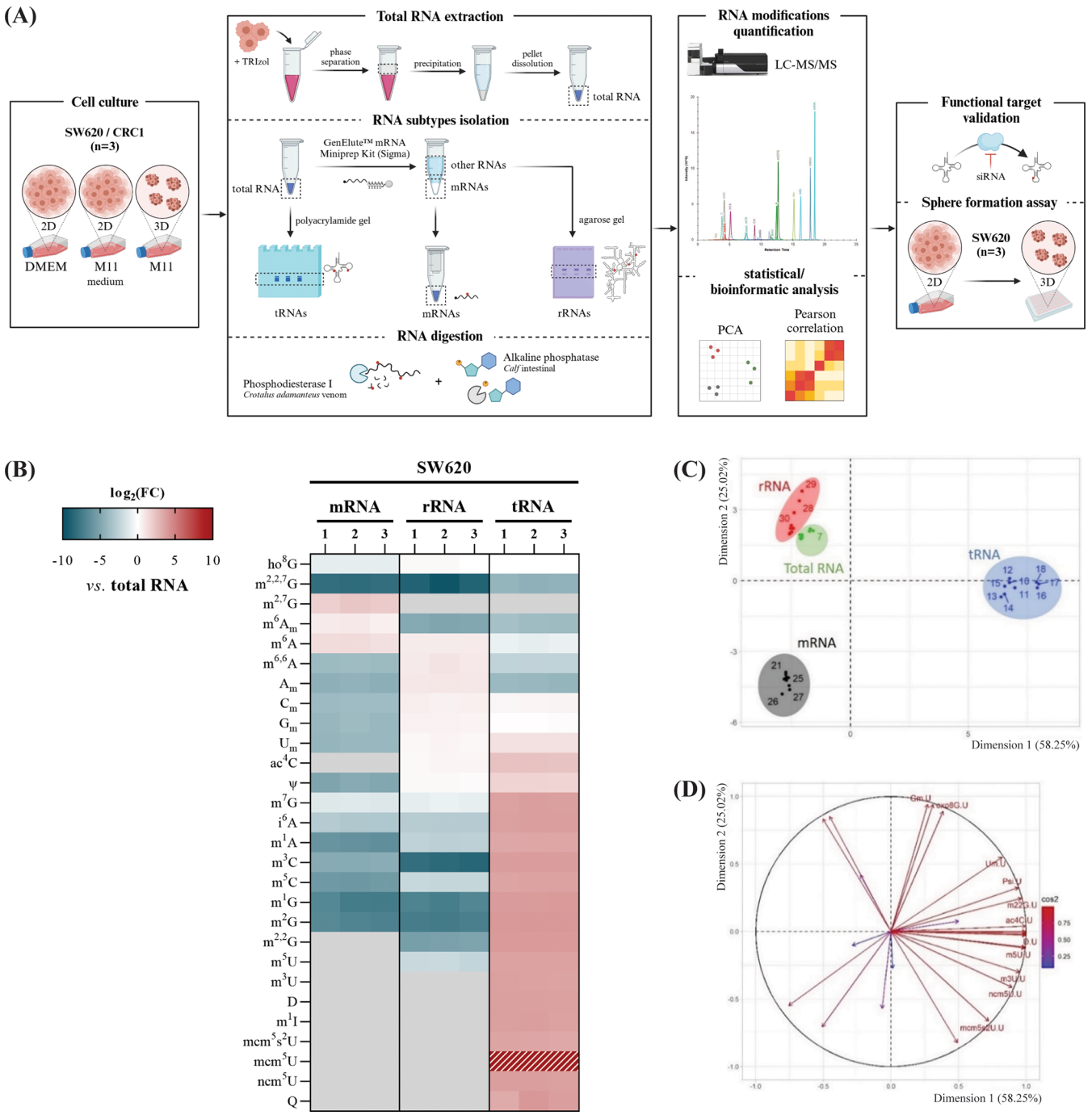


**Figure 1.** RNA modification pattern according to RNA subtypes. (A) Illustration of the experimental pipeline: (1) Culture of cell lines (SW620 and CRC1) in 2D condition (monolayer, DMEM or M11 medium) or 3D condition (suspension culture, M11 medium); (2) total RNA extraction from cells, RNA subtype (mRNA, rRNA, tRNA) isolation, and enzymatic digestion of RNA into nucleosides; (3) injection and analysis by LC-MS/MS followed by statistical/bioinformatic analysis; and (4) functional validation of identified RNA modifications by targeting the corresponding writer(s) (using siRNA) and performing sphere formation assay. (B) Heatmap comparing the modification patterns of mRNA, rRNA, and tRNA with total RNA from SW620 grown in 2D with DMEM ($n$ = 3). A gray box indicates that the nucleoside is not detected, and a hatched box means that it is outside of the $\log_2$(FC) range. (C) Principal component analysis (PCA) of epitranscriptomic profiles from SW620. (D) Graph of variables obtained by PCA of SW620 epitranscriptomic profiles.

majority of RNA marks.[4] Our data clearly establish a correlation between certain RNA modification levels and the enrichment of the corresponding RNA (Figure 1B). For instance, $m^6A$ and $m^6A_m$, which are expected to be mainly present on mRNA,[5] display a high expression level in mRNA samples by contrast with other RNA subtypes, including total RNA samples. $N^7$-methylguanosine ($m^7G$), which is found at the 5′ end of eukaryotic mRNA (cap), displays a lower level in mRNA compared to total RNA. This is simply owing to the fact that this modification is also found in other RNA subtypes like rRNA,[28,29] tRNA,[3] and miRNA.[30] The detection of certain marks in mRNA (such as $m^{6,6}A$, $m^1G$, $m^2G$, and $i^6A$) merely resulted from the presence of contaminants, underlining the limitations of the purification process for this RNA species,


https://doi.org/10.1021/acs.analchem.3c02635
Anal. Chem. 2024, 96, 1825−1833

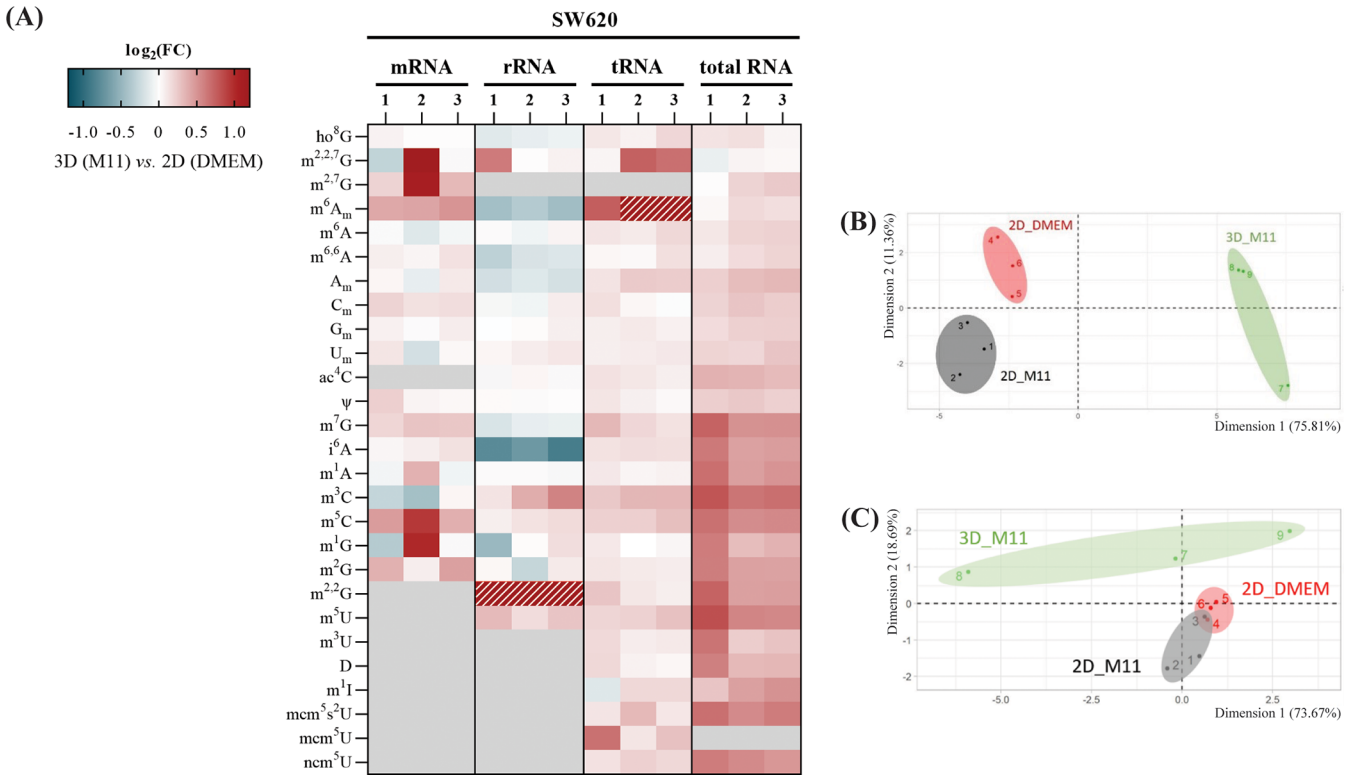


**Figure 2.** Epitranscriptomic landscape evolves along with growth conditions and the cell phenotype. (A) Heatmap comparing the RNA modification profiles of mRNA, rRNA, tRNA, and total RNA from SW620 grown in 3D (M11) versus 2D (DMEM) ($n$ = 3). A gray box indicates that the nucleoside is not detected, and a hatched box means that it is outside of the $\log_2$(FC) range. (B) PCA of epitranscriptomic profiles from SW620 total RNA ($n$ = 3). (C) PCA based on LC-MS/MS analysis of total RNA from CRC1 grown under the three culture conditions and exploiting the minimal signature (eight nucleosides) developed from 2B ($n$ = 3).

which is far less abundant (~4% of the total RNA mass) than tRNA (~15%) and rRNA (~80%).

In rRNA, the most abundant modifications are 2′-O-methylations ($A_m$, $C_m$, $G_m$, $U_m$) and the isomerization of uridine (U) to pseudouridine (Ψ).[31] Therefore, it came as no surprise to detect these modifications in rRNA, as well as in total RNA, which consists primarily of rRNA. As expected, the rRNA-specific modification $N^6$,$N^6$-dimethyladenosine ($m^{6,6}A$) displayed a higher level in rRNA-enriched samples.[32]

Nineteen RNA modifications were mainly detected in tRNA (compared to total RNA). Among them, the 5-carboxy-methyl ($cm^5$) modifications, $ncm^5U$, $mcm^5U$, or $mcm^5s^2U$, are present only at position U34 of 11 tRNA subtypes.[33]

As a control to validate our approach, we sought to evaluate whether epitranscriptomic profiles could easily discriminate among RNA subtypes. In order to model the joint distribution of RNA mark variables, i.e., the variation of individual RNA marks and the correlations between them, we employed PCA (Figure 1C,D). PCA revealed a clear separation of samples according to the RNA subtype, whatever the growth condition (2D or 3D, with DMEM or M11 medium). We could clearly see a distinct separation among total RNA, rRNA (Dimension 1 left, Dimension 2 top), mRNA (Dimension 1 left, Dimension 2 bottom), and tRNA (Dimension 2 right). Remarkably, the high proportion of rRNA in the total RNA samples does not impair their separation. The two represented dimensions account for 83.27% of the explained variance. Eleven quantitative variables were highly correlated ($\cos^2 > 0.95$) with these two dimensions and can represent a minimum pattern to describe the data set (Figure 1D).

In summary, this first series of experiments validated our approach. By combining LC-MS/MS and PCA, we were able to easily isolate and group samples according to RNA subtypes. The RNA subtypes showed characteristic epitranscriptomic profiles, which was to be expected, given that several modified nucleosides, including $m^1A$, $m^5C$, $m^6A$, $m^7G$, $mcms^5S^2U$, and Ψ, are differentially distributed in mRNA, rRNA, and tRNA.[3]

**Global Epitranscriptomic Landscape Evolves in Response to Growth Conditions and Confers Adaptive Properties.** Next, we decided to apply the multiplex analysis of RNA modifications by LC-MS/MS to discriminate between specific cancer cell states. For this purpose, we used three distinct culture media: (1) favorable monolayer growth conditions with serum-enriched medium (named 2D_DMEM); (2) adhesion conditions with serum-deprived medium supplemented with growth hormones (2D_M11); and (3) serum-deprived medium combined with low cell density and the absence of cell adhesion, favoring the CSC phenotype[23] (3D_M11). Serum removal and nonadherent growth conditions exert incremental selection pressure on cancer cells, which must adapt to survive. Using the aforementioned pipeline, we compared the epitranscriptomic landscape of cells grown under these three conditions. As expected, we obtained distinct chemical patterns from one RNA subtype to another (Figure 2A). Independently of the data set, we could clearly separate the culture conditions by PCA (Figures 2B and S11). The epitranscriptomic profiles of total RNA and tRNA samples provided the best separation of culture conditions, with the two dimensions displayed, accounting for 87.17% and 76.01% of the variability in the


https://doi.org/10.1021/acs.analchem.3c02635
Anal. Chem. 2024, 96, 1825−1833

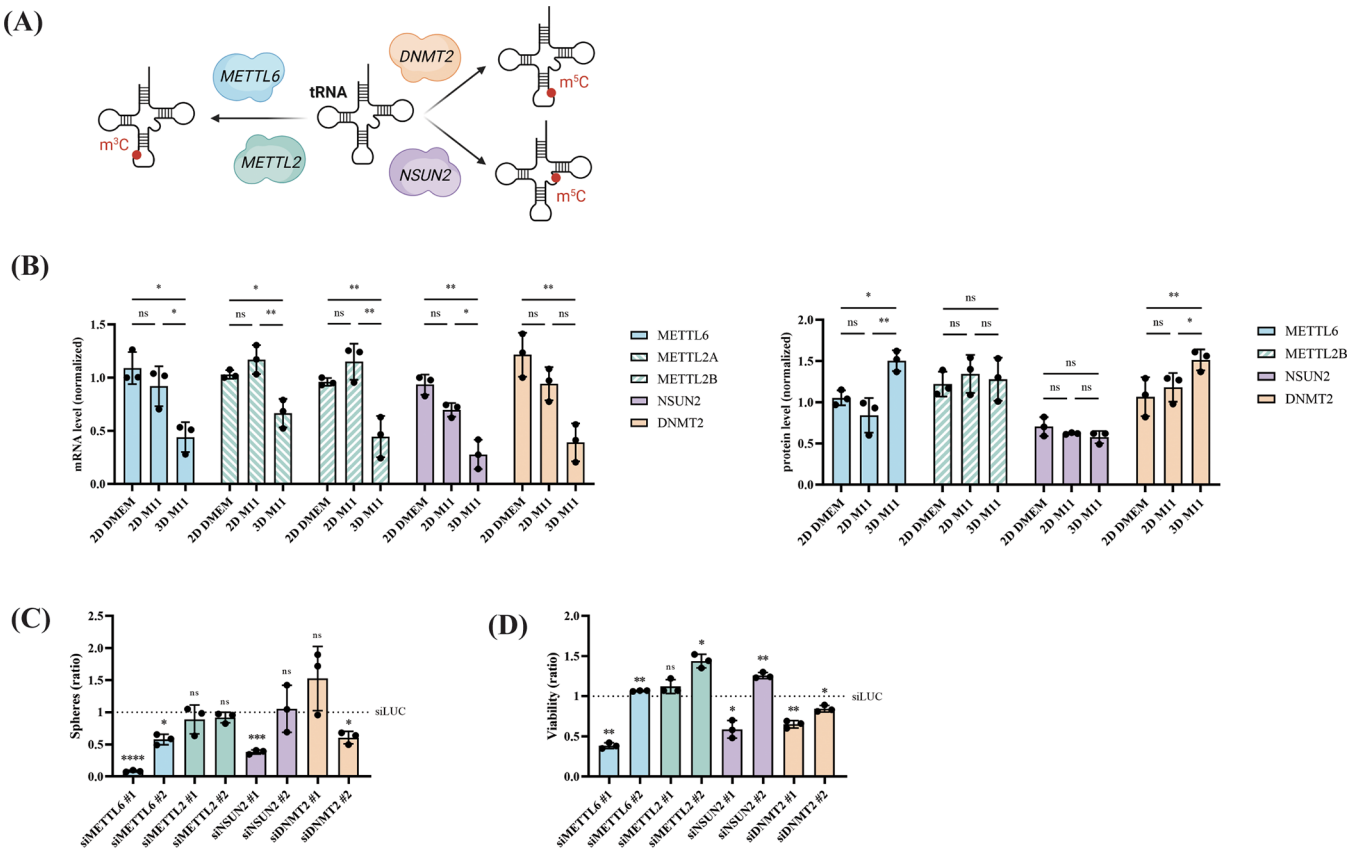


**Figure 3.** Functional validation of identified RNA modifications involved in cell adaptation. (A) Illustration of $m^3C$ and $m^5C$ cytoplasmic tRNA writers. (B) mRNA and protein levels of $m^3C$ and $m^5C$ tRNA methyltransferases in SW620 grown in either 3D (M11) or 2D (DMEM, M11) condition ($n = 3$). One-way analysis of variance (ANOVA), $*p < 0.05$, $**p < 0.005$, $***p < 0.001$, $****p < 0.0001$. (C) Sphere formation assay and (D) cell viability measured by sulforhodamine B assay on SW620 cells transfected with siRNA targeting different methytransferases ($n = 3$). Results are expressed as fold-changes relative to the control (siLUC condition). Welch's $t$ test, $*p < 0.05$, $**p < 0.005$, $***p < 0.001$, $****p < 0.0001$.

data set, respectively. The change in growth medium had a minimal impact on the epitranscriptome (2D_DMEM vs 2D_M11, Figure 2B), as opposed to the transition from monolayer to suspension culture (2D_DMEM vs 3D_M11, Figure 2B). This observation was consistent with the selective advantage conferred by suspension growth to stem-like/progenitor cells.[34] As illustrated in Figure 2A, $m^5C$, $m^3C$, $A_m$, and $m^6A_m$ showed obvious level alterations in both tRNA and total RNA samples.

These results established that isolating a given RNA subtype does not help to discriminate cell status or culture conditions according to the epitranscriptomic profile. Thus, we decided to focus on total RNA analysis in the following section.

PCA with only total RNA separated samples according to culture parameters and in particular, monolayer versus suspension culture (one-dimensional separation with 75.81% of explained variance). Twelve nucleosides, $m^3C$, $ac^4C$, $m^5C$, $ncm^5U$, Ψ, $m^7G$, $m^1A$, $m^2G$, $i^6A$, $m^5U$, $mcm^5s^2U$, and $m^{2,2}G$, were highly correlated with the first dimension ($cos^2 > 0.90$) (Figure S11). To avoid redundancy, a pairwise correlation was also used to identify groups of highly correlated variables (with threshold $|r| > 0.98$) (Figure S12) and keep only the one with the highest $cos^2$ in order to maximize the predictive value of the fewest possible number of variables. Statistical analysis and bioinformatic filtration allowed to establish an "epitranscriptomic signature" consisting of eight nucleosides: {"$m^2G$", "$m^5U$", "$m^3C$", "$ac^4C$", "$m^5C$", "$m^7G$", "$ncm^5U$", "$mcm^5s^2U$"}. These variables enabled separation in the first dimension and constituted an epitranscriptomic signature that distinguishes CSC-enriched culture (3D condition) from control culture (2D condition).

Then, we sought to establish whether this signature was characteristic of a cellular state (or a growth condition), regardless of the genetic background of the cell line. To this end, we reproduced the experiment with another cell line, named CRC1 (Figure S13). CRC1 is significantly different from SW620. SW620 is a commonly used colorectal cancer cell line derived from a metastatic tumor (lymph node) with RAS mutation.[26] The CRC1 cell line was established from a primary tumor (transverse colon), with no detected RAS mutation.[23] Among the eight selected nucleosides from the signature, two were not detected in CRC1 total RNA ($mcm^5S^2U$ and $ncm^5U$), most likely due to lower basal levels in this cell line (Figure S14). Nevertheless, on the basis of the six remaining nucleosides, we were able to clearly separate cell samples according to the culture condition (Figure 2C), thus establishing a link between changes in the epitranscriptomic profile and the adaptation of cancer cells to their growth environment.

Finally, we wanted to validate the functional implications of certain modifications present in the signature. Based on the literature, we focused on $m^5C$ and $m^3C$, two modifications mainly found in tRNAs and potentially involved in the acquisition or maintenance of stem-like properties.[35,36] Four "writers" could be involved in the deposition of these marks on cytoplasmic tRNAs: METTL6, METTL2, DNMT2, and


https://doi.org/10.1021/acs.analchem.3c02635
Anal. Chem. 2024, 96, 1825−1833

NSUN2 (Figure 3A). The quantification of the transcripts encoding these enzymes by quantitative PCR (qPCR) revealed a slight decrease in their expression under suspension culture conditions (Figure 3B). In contrast, protein levels of METTL6 and DNMT2 by immunoblots revealed a significant increase in expression induced by sphere growth (Figures 3B and S15). Targeting these enzymes with siRNA (Figure S16) supported these observations and demonstrated the functional importance of METTL6 ($m^3C$ writer) and DNMT2 ($m^5C$ writer) in the SFA (Figure 3C) while showing a moderate effect on cell viability (Figure 3D).

## CONCLUSIONS

The aim of this study was to conceive a method that could be exploited to identify RNA modifications involved in cancer cell adaptation to inhospitable environments. To this end, we implemented a pipeline combining RNA subtype isolation, LC-MS/MS and statistical analysis, and the functional validation of the identified marks. By comparing distinct cell culture settings, we obtained specific epitranscriptomic profiles as a function of cell growth circumstances or a RNA subtype.

First, the RNA modification profile of a specific RNA subtype was established. Compared with total RNA samples, mRNA, rRNA, and tRNA showed very distinct and characteristic epitranscriptomic profiles. For example, certain modifications are known to be uniquely or predominantly present in certain RNA subtypes, such as $m^6A$ and $m^6A_m$ in mRNA [5], $m^{6,6}A$ in rRNA,[37] and $ncm^5U$, $mcm^5U$, and $mcm^5s^2U$ in tRNA.[33] By simultaneously analyzing 34 RNA modifications in different RNA subtypes, this study confirmed (1) the presence or absence of certain marks in the isolated RNA subtypes and (2) that certain modifications may be present in different RNA subtypes but not with the same abundance.

Based on our results, $m^{2,7}G$ is enriched in mRNA but is detected in neither rRNA nor tRNA. It is known that the $m^7G$ cap can be methylated at the N2 position to give rise to $m^{2,7}G$ and then $m^{2,2,7}G$ [2]. $m^{2,7}G$ could originate from the $m^{2,7}G$ cap ($m^{2,7}GpppN$), whose biological role at the 5′ end of eukaryotic mRNA remains unknown.

Taken individually, the epitranscriptomic profiles of the three main subtypes of RNA (mRNA, rRNA, and tRNA) can distinctly separate SW620 cell culture conditions. tRNA, which is the most extensively modified RNA (13 modifications per molecule on average), gives the most striking separation (Figure S11). In agreement with our previous study,[15] our results show that a global epitranscriptomic profile (based on total RNA) is sufficient to differentiate cell states or culture conditions. Beyond saving experimental time, this simplified procedure offers an additional advantage: isolating total RNA (including RNA fragments) instead of purifying a RNA subtype could prevent a bias triggered by tRNA degradation in frozen samples, as pointed out by Richter et al.[38]

Our study shows that an 8-nucleoside signature {"$m^2G$", "$m^5U$", "$m^3C$", "$ac^4C$", "$m^5C$", "$m^7G$", "$ncm^5U$", "$mcm^5s^2U$"} is sufficient to effectively distinguish cell samples/state according to their growth condition. Remarkably, the epitranscriptomic signature established from SW620 sample analysis also enabled CRC1 samples to be discriminated according to the culture condition. This result suggests the involvement of these modifications in cell adaptation to suspension growth, associated with stemlike properties. The impact of certain RNA mark players on stem cell capacities was previously studied, like (tRNA) pseudouridine synthase PUS7 in glioblastoma stem cells,[39] (mRNA) $N^4$-acetyltransferase NAT10 in bladder cancer stem cells,[40] (tRNA) $m^1A$ methyltransferase TRMT6/TRMT61A in liver cancer stem cells,[41] and (tRNA) $m^7G$ methyltransferase METTL1 in human-induced pluripotent stem cells.[42] In this study, we focused our attention on $m^5C$ and $m^3C$, both enriched in tRNA and present in the 8-nucleoside signature. Discrepancies between qPCR and immunoblot (as well as LC-MS/MS) results confirmed that it is preferable to track the product of enzyme activity rather than relying on simple quantification of the transcripts encoding the enzymes. DNMT2 catalyzes the methylation of the C38 position in the anticodon loop of tRNAs, in particular $tRNA^{Asp}$, its most common substrate.[43] The methylation of position C38 in $tRNA^{Asp}$ stimulates their loading *in vivo* and *in vitro*, therefore promoting the translation of proteins with a multitude of Asp.[44] C38 methylation is also involved in tRNA stability under stress conditions[45] and the regulation of translational fidelity.[46] In the context of (cancer) stem cell biology, $m^5C$ has been shown to regulate the balance of stem and progenitor epidermal or neural cells by controlling tRNA cleavage.[36] METTL6 catalyzes the C32 $m^3C$ formation of specific serine tRNA isoacceptors. It has an impact in mRNA translation and could modulate the self-renewal and pluripotency potential of stem cells, including hepatocellular carcinoma cells.[35] As a result, both DNMT2 and METTL6 may influence the post-transcriptional expression of key genes for stem-like properties and sphere formation in colorectal cell lines.

To conclude, our study shows that the use of total RNA and a small number of nucleosides (<10) is sufficient to distinctly separate samples according to the culture condition or the cell state. This method could be exploited to identify RNA marks potentially involved in cell adaptation to a given stress, culture condition, or tissue environment. We have identified RNA marks ($m^5C$ and $m^3C$ in particular) associated with the SFA, often correlated with the acquisition of the CSC phenotype. Ongoing investigations will determine the role of these modifications on stem-like properties, like chemoresistance and tumor initiation, in the context of colorectal cancer. This could pave the way for the identification of therapeutic targets among epitranscriptomic effectors,[47] whose inhibition could cripple CSC adaptation and prevent chemoresistance and metastasis.

## ASSOCIATED CONTENT

### Supporting Information

The Supporting Information is available free of charge at https://pubs.acs.org/doi/10.1021/acs.analchem.3c02635.

Primer sequences used to perform qPCR analysis; MS/MS parameters for MRM analysis of nucleosides; calibration curves for all nucleosides in the standard mix; signature selection algorithm; list of antibodies to perform WB; siRNA sequences; RNA quantification; acrylamide gels; agarose gels; qPCR analysis on RNA subtypes; graph of individuals and variables of epitranscriptomic profiles from mRNA, rRNA, or tRNA of SW620; graph of variables of epitranscriptomic profiles from total RNA of SW620; heatmap comparing the modification patterns of mRNA, rRNA, and tRNA to total RNA from CRC1, cultured in 2D with DMEM; linear correlation coefficient between each pair of marks



https://doi.org/10.1021/acs.analchem.3c02635
Anal. Chem. 2024, 96, 1825−1833

and variation among the 9 samples; WB blots; and qPCR analysis after siRNA transfection (PDF)

## AUTHOR INFORMATION


### Corresponding Authors

**Christophe Hirtz** − *IRMB-PPC, INM, CHU Montpellier, INSERM, Université de Montpellier, CNRS, 34090 Montpellier, France;* orcid.org/0000-0002-7313-0629; Email: christophe.hirtz@umontpellier.fr

**Alexandre David** − *IGF, INSERM and IRMB-PPC, INM, CHU Montpellier, INSERM, Université de Montpellier, CNRS, 34090 Montpellier, France;* orcid.org/0000-0003-3365-1339; Email: alexandre.david@inserm.fr

### Authors

**Amandine Amalric** − *IGF, INSERM and IRMB-PPC, INM, CHU Montpellier, INSERM, Université de Montpellier, CNRS, 34090 Montpellier, France;* orcid.org/0000-0002-2856-1446

**Aurore Attina** − *IRMB-PPC, INM, CHU Montpellier, INSERM, Université de Montpellier, CNRS, 34090 Montpellier, France*

**Amandine Bastide** − *IGF, INSERM, Université de Montpellier, CNRS, 34090 Montpellier, France;* orcid.org/0000-0001-7896-8490

**Marion Buffard** − *IGF, INSERM and LIRMM, Université de Montpellier, CNRS, 34090 Montpellier, France*

**Stéphanie Mateus** − *IGF, INSERM, Université de Montpellier, CNRS, 34090 Montpellier, France*

**Chris Planque** − *IGF, INSERM, Université de Montpellier, CNRS, 34090 Montpellier, France*

**Eric Rivals** − *LIRMM, Université de Montpellier, CNRS, 34090 Montpellier, France;* orcid.org/0000-0003-3791-3973

Complete contact information is available at: https://pubs.acs.org/10.1021/acs.analchem.3c02635


### Author Contributions

[‖]A. Amalric and A. Attina contributed equally to this paper. A.D., E.R., A.B., A. Amalric, and A. Attina designed the experiments and analyzed the results. A. Amalric, A. Attina, S.M., and C.P. performed the experiments. A. Amalric, A. Attina, E.R., A.D., C.H., and A.B. performed data analyses. M.B., A. Attina, and E.R. designed and performed bioinformatics analysis. A.D., A. Amalric, A. Attina, and C.H. wrote the manuscript. All authors reviewed the final version of the manuscript.

### Notes

The authors declare no competing financial interest.

## ACKNOWLEDGMENTS

Our teams were generously supported by Occitanie Region/FEDER (PPRi, SMART Project), (RPT20001FFA − INCA 2020-116), Fondation ARC (ARCDOC42022010004641), Ligue Contre le Cancer (No. AAPARN 2022.LCC/AID), and i-site MUSE (LabMUSE EpiGenMed). Mass spectrometry experiments were carried out using the facilities of the Montpellier Proteomics Platform (PPM-PPC, BioCampus Montpellier).

## REFERENCES


(1) Bhatti, G. K.; Khullar, N.; Sidhu, I. S.; Navik, U. S.; Reddy, A. P.; Reddy, P. H.; Bhatti, J. S. *Metab. Brain Dis.* **2021**, *36* (6), 1119−1134.

(2) Boccaletto, P.; Stefaniak, F.; Ray, A.; Cappannini, A.; Mukherjee, S.; Purta, E.; Kurkowska, M.; Shirvanizadeh, N.; Destefanis, E.; Groza, P.; Avşar, G.; Romitelli, A.; Pir, P.; Dassi, E.; Conticello, S. G.; Aguilo, F.; Bujnicki, J. M. *Nucleic Acids Res.* **2022**, *50* (D1), D231−D235.

(3) Barbieri, I.; Kouzarides, T. *Nat. Rev. Cancer* **2020**, *20*, 303.

(4) Suzuki, T. *Nat. Rev. Mol. Cell Biol.* **2021**, *22* (6), 375−392.

(5) Song, J.; Yi, C. *J. Mol. Biol.* **2020**, *432* (6), 1824−1839.

(6) Sharma, S.; Lafontaine, D. L. J. *Trends Biochem. Sci.* **2015**, *40* (10), 560−575.

(7) Roundtree, I. A.; Evans, M. E.; Pan, T.; He, C. *Cell* **2017**, *169* (7), 1187−1200.

(8) Uddin, M. B.; Wang, Z.; Yang, C. *Theranostics* **2020**, *10* (7), 3164−3189.

(9) Takeshima, H.; Ushijima, T. *npj Precis. Oncol.* **2019**, *3* (1), 7.

(10) Walther, A.; Johnstone, E.; Swanton, C.; Midgley, R.; Tomlinson, I.; Kerr, D. *Nat. Rev. Cancer* **2009**, *9* (7), 489−499.

(11) Ruiz-Bañobre, J.; Goel, A. Genomic and Epigenomic Biomarkers in Colorectal Cancer: From Diagnosis to Therapy. In *Advances in Cancer Research*; Berger, F. G.; Boland, C. R., Eds.; Academic Press, 2021; Vol. *151*, Chapter 7, pp 231−304.

(12) Martins, B. A. A.; de Bulhões, G. F.; Cavalcanti, I. N.; Martins, M. M.; de Oliveira, P. G.; Martins, A. M. A. *Front. Oncol.* **2019**, *9*, No. 1284, DOI: 10.3389/fonc.2019.01284.

(13) Rachiglio, A. M.; Sacco, A.; Forgione, L.; Esposito, C.; Chicchinelli, N.; Normanno, N. *Explor. Targeted Antitumor Ther.* **2020**, *1* (1), 53−70.

(14) Amalric, A.; Bastide, A.; Attina, A.; Choquet, A.; Vialaret, J.; Lehmann, S.; David, A.; Hirtz, C. *Crit Rev. Clin. Lab. Sci.* **2022**, *59* (1), 1−18.

(15) Relier, S.; Amalric, A.; Attina, A.; Koumare, I. B.; Rigau, V.; Burel Vandenbos, F.; Fontaine, D.; Baroncini, M.; Hugnot, J. P.; Duffau, H.; Bauchet, L.; Hirtz, C.; Rivals, E.; David, A. *Anal. Chem.* **2022**, *94*, 11967.

(16) Nombela, P.; Miguel-López, B.; Blanco, S. *Mol. Cancer* **2021**, *20*, 18.

(17) Liu, S.; Chen, S.; Tang, C.; Zhao, Y.; Cui, W.; Jia, L.; Wang, L. *Front. Oncol.* **2022**, *12*, No. 970833.

(18) Zhao, K.; Li, W.; Yang, Y.; Hu, X.; Dai, Y.; Huang, M.; Luo, J.; Zhang, K.; Zhao, N. *Front. Immunol.* **2022**, *13*, No. 955848.

(19) Zhang, H.; Fu, H.; Fang, H.; Deng, Q.; Huang, H.; Hou, D.; Wang, M.; Yao, Q.; Si, Q.; Chen, R.; Li, L.; Weng, J.; Guo, T.; Wang, M. *Stem Cells Int.* **2022**, *2022*, No. 5015856.

(20) Li, M.; Tao, Z.; Zhao, Y.; Li, L.; Zheng, J.; Li, Z.; Chen, X. *J. Transl. Med.* **2022**, *20*, 214.

(21) Song, H.; Zhang, J.; Liu, B.; Xu, J.; Cai, B.; Yang, H.; Straube, J.; Yu, X.; Ma, T. *Biomark. Res.* **2022**, *10*, 15.

(22) Yang, B.; Wang, J.-Q.; Tan, Y.; Yuan, R.; Chen, Z.-S.; Zou, C. *Pharmacol. Res.* **2021**, *174*, No. 105937.

(23) Relier, S.; Ripoll, J.; Guillorit, H.; Amalric, A.; Achour, C.; Boissière, F.; Vialaret, J.; Attina, A.; Debart, F.; Choquet, A.; Macari, F.; Marchand, V.; Motorin, Y.; Samalin, E.; Vasseur, J.-J.; Pannequin, J.; Aguilo, F.; Lopez-Crapez, E.; Hirtz, C.; Rivals, E.; Bastide, A.; David, A. *Nat. Commun.* **2021**, *12*, No. 1716.

(24) Thomas, J. M.; Batista, P. J.; Meier, J. L. *ACS Chem. Biol.* **2019**, *14* (3), 316−324.

(25) Atashzar, M. R.; Baharlou, R.; Karami, J.; Abdollahi, H.; Rezaei, R.; Pourramezan, F.; Zoljalali Moghaddam, S. H. *J. Cell. Physiol.* **2020**, *235* (2), 790−803.

(26) Leibovitz, A.; Stinson, J. C.; McCombs, W. B.; McCoy, C. E.; Mazur, K. C.; Mabry, N. D. *Cancer Res.* **1976**, *36* (12), 4562−4569.

(27) Lê, S.; Josse, J.; Husson, F. *J. Stat. Software* **2008**, *25*, 1−18, DOI: 10.18637/jss.v025.i01.

(28) Haag, S.; Kretschmer, J.; Bohnsack, M. T. *RNA* **2015**, *21* (2), 180−187.

(29) Zorbas, C.; Nicolas, E.; Wacheul, L.; Huvelle, E.; Heurgué-Hamard, V.; Lafontaine, D. L. J. *Mol. Biol. Cell* **2015**, *26* (11), 2080−2095.
(30) Pandolfini, L.; Barbieri, I.; Bannister, A. J.; Hendrick, A.; Andrews, B.; Webster, N.; Murat, P.; Mach, P.; Brandi, R.; Robson, S. C.; Migliori, V.; Alendar, A.; d'Onofrio, M.; Balasubramanian, S.; Kouzarides, T. *Mol. Cell* **2019**, *74* (6), 1278−1290.
(31) Sloan, K. E.; Warda, A. S.; Sharma, S.; Entian, K.-D.; Lafontaine, D. L. J.; Bohnsack, M. T. *RNA Biol.* **2017**, *14* (9), 1138−1152.
(32) Liu, C.; Cao, J.; Zhang, H.; Yin, J. *Biology* **2022**, *11* (2), 214.
(33) Hawer, H.; Hammermeister, A.; Ravichandran, K. E.; Glatt, S.; Schaffrath, R.; Klassen, R. *Genes* **2019**, *10* (1), 19.
(34) Liu, J. C.; Deng, T.; Lehal, R. S.; Kim, J.; Zacksenhaus, E. *Cancer Res.* **2007**, *67* (18), 8671−8681.
(35) Ignatova, V. V.; Kaiser, S.; Ho, J. S. Y.; Bing, X.; Stolz, P.; Tan, Y. X.; Lee, C. L.; Gay, F. P. H.; Lastres, P. R.; Gerlini, R.; Rathkolb, B.; Aguilar-Pimentel, A.; Sanz-Moreno, A.; Klein-Rodewald, T.; Calzada-Wack, J.; Ibragimov, E.; Valenta, M.; Lukauskas, S.; Pavesi, A.; Marschall, S.; Leuchtenberger, S.; Fuchs, H.; Gailus-Durner, V.; de Angelis, M. H.; Bultmann, S.; Rando, O. J.; Guccione, E.; Kellner, S. M.; Schneider, R. *Sci. Adv.* **2020**, *6* (35), No. eaaz4551.
(36) Guzzi, N.; Bellodi, C. *RNA Biol.* **2020**, *17* (8), 1214−1222, DOI: 10.1080/15476286.2020.1732694.
(37) Natchiar, S. K.; Myasnikov, A. G.; Kratzat, H.; Hazemann, I.; Klaholz, B. P. *Nature* **2017**, *551* (7681), 472−477.
(38) Richter, F.; Plehn, J. E.; Bessler, L.; Hertler, J.; Jörg, M.; Cirzi, C.; Tuorto, F.; Friedland, K.; Helm, M. *Nucleic Acids Res.* **2021**, *50*, 4201−4215, DOI: 10.1093/nar/gkab1150.
(39) Cui, Q.; Yin, K.; Zhang, X.; Ye, P.; Chen, X.; Chao, J.; Meng, H.; Wei, J.; Daniel, R.; Li, L.; Qin, Y.; Sun, G.; Zhang, M.; Klein, J.; Huynhle, M.; Wang, C.; Zhang, L.; Badie, B.; Kalkum, M.; He, C.; Yi, C.; Shi, Y. *Nat. Cancer* **2021**, *2* (9), 932−949.
(40) Wang, G.; Zhang, M.; Zhang, Y.; Xie, Y.; Zou, J.; Zhong, J.; Zheng, Z.; Zhou, X.; Zheng, Y.; Chen, B.; Liu, C. *Clin. Transl. Med.* **2022**, *12* (5), No. e738.
(41) Wang, Y.; Wang, J.; Li, X.; Xiong, X.; Wang, J.; Zhou, Z.; Zhu, X.; Gu, Y.; Dominissini, D.; He, L.; Tian, Y.; Yi, C.; Fan, Z. *Nat. Commun.* **2021**, *12*, No. 6314.
(42) Deng, Y.; Zhou, Z.; Ji, W.; Lin, S.; Wang, M. *Stem Cell Res. Ther.* **2020**, *11*, 306.
(43) Goll, M. G.; Kirpekar, F.; Maggert, K. A.; Yoder, J. A.; Hsieh, C.-L.; Zhang, X.; Golic, K. G.; Jacobsen, S. E.; Bestor, T. H. *Science* **2006**, *311* (5759), 395−398.
(44) Shanmugam, R.; Fierer, J.; Kaiser, S.; Helm, M.; Jurkowski, T. P.; Jeltsch, A. *Cell Discovery* **2015**, *1* (1), 15010.
(45) Schaefer, M.; Pollex, T.; Hanna, K.; Tuorto, F.; Meusburger, M.; Helm, M.; Lyko, F. *Genes Dev.* **2010**, *24* (15), 1590−1595.
(46) Tuorto, F.; Herbst, F.; Alerasool, N.; Bender, S.; Popp, O.; Federico, G.; Reitter, S.; Liebers, R.; Stoecklin, G.; Gröne, H.-J.; Dittmar, G.; Glimm, H.; Lyko, F. *EMBO J.* **2015**, *34* (18), 2350−2362.
(47) Berdasco, M.; Esteller, M. *Br. J. Pharmacol.* **2022**, *179*, 2868−2889, DOI: 10.1111/bph.15604.


https://doi.org/10.1021/acs.analchem.3c02635
*Anal. Chem.* 2024, 96, 1825−1833